



Finite Element Modelling of Creep Rupture on Grade 91 Steel using Monkman-Grant Ductility based Damage Model

N.A. Alang^{1*}, J. Alias², Z. Sajuri³, S. Nur Atiqah¹

¹Structural Performance and Materials Engineering (SUPREME), Faculty of Mechanical and Automotive Engineering Technology, Universiti Malaysia Pahang, 26600, Pekan, Pahang, MALAYSIA

²Department of Mechanical Engineering, College of Engineering, Universiti Malaysia Pahang, 26300, Kuantan, Pahang, MALAYSIA

³Centre for Materials Engineering and Smart Manufacturing (MERCU), Faculty of Engineering and Built Environment, Universiti Kebangsaan Malaysia, Selangor, 43650, MALAYSIA

*Corresponding Author

DOI: <https://doi.org/10.30880/ijie.2021.13.07.014>

Received 16 August 2021; Accepted 2 September 2021; Available online 30 September 2021

Abstract: Failure strain is a main parameter used in the ductility exhaustion based damage model in which the accuracy of the prediction is dependent on its input value. The experimental measured has indicated that the value of strain at fracture is extensively scattered, therefore may affect the prediction. This paper presents the result of creep rupture time using a modified creep damage model incorporating Monkman-Grant (MG) failure strain as an alternative to strain at fracture. Both strains at fracture and MG failure strain are separately employed in the damage model to predict the failure time of uniaxial smooth specimen and notched bar with different acuity ratios of 3.0 and 20. The FE model of the specimen is loaded under different stress values and the multiaxial failure strain at each stress level is estimated using Cock and Ashby void growth model. The predicted creep rupture time that is compared to the experimental data (in a range of 40-1000 hours) showing a good agreement within the scatter band of +/- factor of 2. Both approaches using strain at fracture and MG failure strain can be used in predicting the creep failure under uniaxial and multiaxial features. The advantage of using MG strain is that the laboratory creep testing can be interrupted prior to specimen fractured or once the secondary creep deformation occurs. Meanwhile, the determination of strain at fracture needs longer test duration where the test can be stopped only when the specimen broken.

Keywords: Creep, damage, grade 91 steel, multiaxial stress state, rupture

1. Introduction

Grade 91 steel is used widely as a component in nuclear and fossil power plants due to its excellent mechanical and creep properties especially at high temperature. The material is subjected to creep damage after long-term in service, resulting in the breakdown or degradation in creep strength [1]. The components made from this material experience local multiaxial stress state due to internal microscopic damage as well as global multiaxial stress state due to geometrical change. Notched bar specimens are extensively used in the laboratory to investigate the effect of various stress states on creep deformation and rupture behavior of materials. By adjusting the notch radius, different stress states can be achieved. The creeping component's residual service life is often evaluated using two key predictive methods: the life fracture rule [2] and ductility- (or strain) based models. In general, the life fracture rule can be written as:

$$\omega = \sum \frac{t_n}{t_{r_n}} \tag{1}$$

where t_n denotes the in-service duration and t_{r_n} is the time to rupture. Since the stress at the gauge area is unchanged and the same as the applied stress, determining the time to rupture for a uniaxial sample is straightforward. However, for a notched bar sample, selecting the right stress is crucial as the stress and creep strain distribution at the notched area is non-uniform and somewhat complex. When applied to a multiaxial state of stress, such as a notched bar sample, equation (1) can lead to conservative predictions.

Numbers of researchers [3–5] employed the model which has been derived based on Continuum Damage Mechanics (CDM) concept to predict rupture time of the component under multiaxial stress state condition. CDM model which incorporates various parameter and material constants to describe the coarsening of precipitates as well as intergranular creep constrained cavitation damage, aging and strain hardening effect has been proposed, however the model is generally complex. The accuracy of the prediction is also strongly depending on the derived material constants of the model. The determination of material constant is not an easy and straightforward process. A set of complete creep deformation behavior of different stress levels is usually required to determine the model parameters. In fact, robust optimization technique or algorithm is required to fit the constitutive equations to the experimental creep data. With different service conditions and batch-to-batch creep property variance, adding difficulty in the analysis of determining material constants.

The use of ductility exhaustion model coupled with FE gives a satisfactory prediction of creep rupture time under various states of stress conditions. In order to account the creep deformation in all stages, the average creep strain rate has been used by many researchers [6,7]. The corresponding strain or strain at failure then is chosen to be substituted into the damage model. For the sample with notches or irregularity, the multiaxial failure strain is required to perform the prediction. However, determination of this strain in laboratory is not straightforward, thus it is usually estimated using void growth models [8–10]. These models relate between the two parameters; multiaxial-to-uniaxial ratio and triaxiality ratio, h . The relation suggested by the models is consistent at triaxiality ratio of $h = 0.33$ (as in uniaxial sample), however, deviates between each other when the h increases. To address the above mentioned issue, Alang et al. [11] derived a simple relation between the two parameters by taking the average value from several void growth models.

Despite the fact that a good prediction was obtained when strain at fracture was utilized, laboratory measurements have indicated that strain at fracture values are significantly scattered. This implies to the creep deformation that occurs at the outset of a fracture is unstable. In fact, due to the variation in heat-to-heat, chemical composition, and material condition; as-received or ex-service, the data published in the literature [12,13] is also shows some degree of discrepancy. It is likely, better prediction can be obtained when pedigree data is being used and upper and lower bounds of data scatter are taking into account. In another studies, it has been reported that employing strain at fracture also leads to conservative result particularly for high notch acuity (or sharp notch) [14]. Alternatively, Monkman-Grant strain has shown better stability in the value [11] because it is measured during uniform deformation or secondary stage, thus is not affected by the tensile instability or necking that usually occur during tertiary creep. Under creep environment, the Grade 91 steel exhibits longer secondary deformation and spent most of its life in this region. Thus, there is a potential to use MG strain as an alternative to the strain at failure. Fig. 1 defines several parameters used in this study.

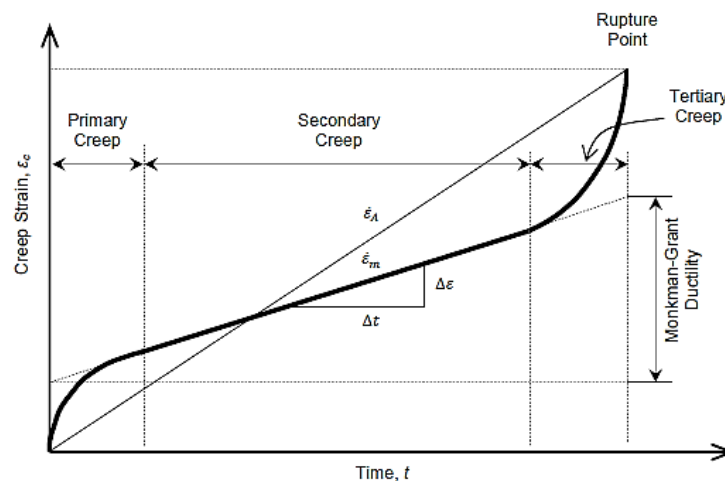


Fig. 1 - Definition of various parameters in creep curve

This study intends to numerically assess the ability of the MG failure strain as a key parameter in the ductility exhaustion-based damage model to predict creep rupture time of Grade 91 steel under various stress state levels. The feasibility of replacing strain at fracture with MG strain in damage model will be examined.

2. Material and Damage Models

2.1 Constitutive Material Model

The elastic-plastic-creep material models were employed in the simulation. The total strain of the material under creep condition is given by the summation of elastic and inelastic (plastic and creep) components.

$$\epsilon_T = \epsilon_e + \epsilon_p + \epsilon_c \tag{2}$$

The elastic strain is assumed to obey the Hooke’s Law while plastic strain is assumed to follow the power law relation. Table 1 tabulates the elastic-plastic mechanical properties of Grade 91 steel.

$$\sigma_p = K(\epsilon_p)^N \tag{3}$$

where, K is power hardening coefficient and N is the strain hardening exponent.

Table 1 - Elastic-plastic mechanical properties of Grade 91 steel [15]

E (GPa)	K (MPa)	N
164	673.9	0.16

The uniaxial creep deformation data at 600°C that is used to determine the material constant of material and the damage models were taken from [16]. A total of 69 data points which covers both short- and long-term time (up to 87,000 hours test duration) are analyzed. Note that the specimen used for the experimental testing was extracted from plate, tube and pipe of Grade 91 steel that was having slightly different chemical composition. Due to this reason, a certain level of data scatter is anticipated. The determination of material constant (of the models), is based on the best fit curve.

Fig. 2 shows the plot (in log-log scale) of minimum and average creep strain rate against stress of uniaxial creep sample. Both figures show the same data trend where the data can be represented by bi-linear line with a different slope. The turning point of both slopes at 0.5 of yield strength, S_y (approximately, $\sigma = 125$ MPa) can be clearly seen, indicating the different in creep deformation mechanisms. The value consistent to other advanced ferritic creep resistant steels as reported by Kimura et al. [17]. At high stress, the dislocation or often called power law creep is dominant and governs the creep deformation. Dislocation can move by gliding in a slip plane or climbing with the aid of diffusion. Meanwhile, at low stress, the diffusional process dominates [18]. The different of creep process dominant caused the two slopes of the data. It is found that Grade 92 steel is also exhibits the same trend at different temperature levels [19]. Based on Figs. 2 and 3, the data for both minimum and average creep strain rate can be fitted using the two linear or bi-linear Norton power law relation:

$$\dot{\epsilon} = A\sigma^n \begin{cases} A = A_s \text{ or } (A_s)_{ave} & \text{and } n = n_s \text{ or } (n_s)_{ave} & \text{if } \sigma > 0.5S_y \\ A = A_L \text{ or } (A_L)_{ave} & \text{and } n = n_L \text{ or } (n_L)_{ave} & \text{if } \sigma \leq 0.5S_y \end{cases} \tag{4}$$

The value of A and n are presented in Fig. 2. Short-term and long-term creep is denoted by the letters S and L , respectively. It is clearly shown that at long term creep, material deforms at faster rate compared to the estimation rate by extrapolation data from short-term time. It indicated that using the short- term data to predict long-term behavior tends to overestimate the creep life. Due to the reason, careful precaution should be taken when only short-term data is available. The stress of 125 MPa (at turning point between two creep deformation mechanisms) is employed in FE as a boundary between short-and long-term creep.

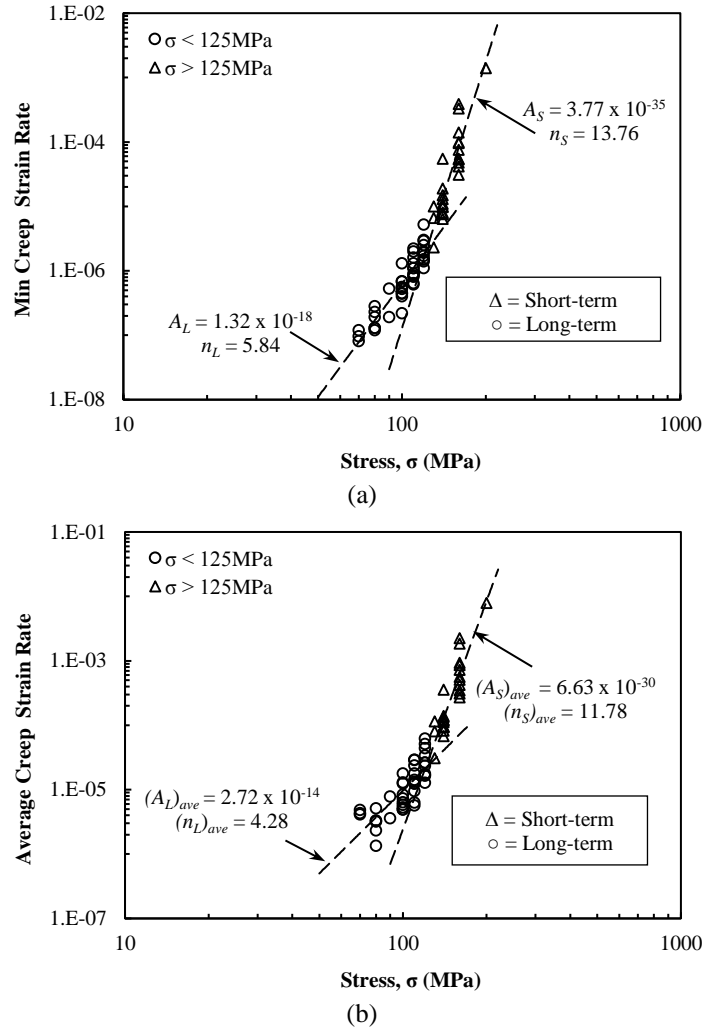


Fig. 2 - Creep strain rate against stress (a) minimum; (b) average

2.2 Damage Model

One of the well-known methods to predict the creep life is based on the ductility exhaustion damage model. The failure is assumed to occur when the accumulated creep strain reaches the critical strain. Creep damage rate, $\dot{\omega}$ is defined by the ratio of creep strain rate, $\dot{\epsilon}_c$ and multiaxial creep ductility, ϵ_f^* . The damage accumulated at time, t is calculated using simple integration rule as given in equation (5):

$$\omega = \int_0^t \dot{\omega} dt = \int_0^t \frac{\dot{\epsilon}_c}{\epsilon_f^*} \quad (5)$$

Local failure is assumed to occur when the damage parameter, ω of the element approaches 0.99. At this point, the progressive creep damage is simulated by simply reducing the elastic modulus to a very minimal number. In present simulation, it is reduced 99% from the original value. The user subroutine USDFLD is used in ABAQUS to implement the progressive damage modelling technique mentioned above. Note that the value of multi-axial creep ductility in equation (5) depends on the uniaxial creep ductility and stress triaxiality (the ratio of mean principle stresses, σ_m and equivalent stress, σ_e). The well-known model that defines between these parameters is given by [10] in equation (6):

$$\frac{\epsilon_f^*}{\epsilon_f} = \sinh \left[\frac{2}{3} \left(\frac{n-0.5}{n+0.5} \right) \right] / \sinh \left[2 \left(\frac{n-0.5}{n+0.5} \right) \frac{\sigma_m}{\sigma_e} \right] \quad (6)$$

The uniaxial failure strain (MG failure strain and strain at failure) is shown to be stress or strain rate dependent. The difference in controlled failure mechanisms between short- and long-term creep is demonstrated by the decline in failure

strain over creep duration. To fitting the failure strain data from high to low stress regimes, a single function describing failure strain as a function of creep strain rate is employed and mathematically can be written as:

$$\epsilon_f = f(\dot{\epsilon}_c) = \frac{\epsilon_{f_{max}} + \epsilon_{f_{min}} \left(\frac{\dot{\epsilon}_c}{\dot{\epsilon}}\right)^{-\alpha}}{\left(\frac{\dot{\epsilon}_c}{\dot{\epsilon}}\right)^{-\alpha} + 1} \quad (7)$$

Using equation (7), the strain at fracture against strain rate of Grade 91 steel is plotted and show significant dependency between two parameters. Similar trend is also observed when the strain at fracture is replaced by the Monkman-Grant failure strain. This behavior is consistent with the trends obtained from the void growth models where at high stress the failure strain is controlled by the plastic deformation and independent to the strain rate. As a strain rate decreases, the diffusion-controlled void growth takes place. As a result, the failure strain reduces as the strain rate slower. At low stress levels or very long-term creep time, cavitation is expected to be heterogeneous, and the creep deformation of the non-cavitated areas is slow enough to constrain the diffusion growth of inter-granular cavities. The constrained diffusion cavity growth also predicts that creep ductility is insensitive to the strain rate [20]. Table 2 and 3 tabulate the value of parameter according to equation (7) for Grade 91 steel. It is worth to note that the plateau value of minimum creep failure strain is not clearly observed due to the limited availability of the long-term creep data. The $\epsilon_{f_{min}}$, therefore is assumed to have the value of 5% from the $\epsilon_{f_{max}}$.

Table 2 - Fehmi's equation constant for Monkman Grant failure strain against strain rate plot

$\epsilon_{f_{max}}$	$\epsilon_{f_{min}}$	α	$\dot{\epsilon}$
0.06	0.003	0.5	9.00×10^{-6}

Table 3 - Fehmi's equation constant for strain at fracture against strain rate plot

$\epsilon_{f_{max}}$	$\epsilon_{f_{min}}$	α	$\dot{\epsilon}$
0.38	0.019	0.6	5.65×10^{-6}

The failure strain at rupture has been given more emphasis as a damage parameter compared to MG failure strain. The advantage of using failure strain at rupture is that the accumulation strain at all creep stages (primary, secondary and tertiary) is accounted for. However, failure strain at rupture show considerably scatters since the value is greatly influenced by the unstable process of fracture during the tertiary stage of creep deformation due to plasticity especially at high stress level. In addition, the material experiences multiaxial stress state which attributed to the so-called 'necking' phenomenon during tertiary deformation. Unlike MG failure strain, its value is measured during the secondary stage in which the material deforms uniformly so that the uniaxial stress state condition is preserved.

2.3 Finite Element Modelling

Smooth, U- and V-type notched bar is modeled in FE commercial FE package ABAQUS v6.14 as an axis-symmetric due to geometrical and loading symmetric. Only a quarter of the specimen is modelled. The necessary boundary condition (Fig. 3) is applied to simulate the symmetric condition. The prescribed load/stress is assigned to the top surface of the sample. Note that the asterisk '*' represents for V-type notched bar. The smooth bar has a diameter of 8 mm and gauge length of 36 mm. The notched bar has the same gauge length and gross diameter as in smooth bar. The net diameter or ligament is kept constant at 5.7 mm. Since the smooth bar's cross-section area is uniform throughout its gauge length, the stress distribution within this area is insensitive to the mesh size and number of mesh. Therefore, courser mesh size has been used to reduce the computational time. However, a sufficiently small mesh size is assigned for notched sample, particularly around the notch area where the stress gradient is usually observed. The number of elements designed to the uniaxial sample is 96. For the notched bar, a 2100-2400 nodes and 2200-2540 elements are assigned. The continuum axis-symmetric quadrilateral elements with reduced integration scheme (CAX4R) are assigned. The details of FE structured mesh are shown in Fig. 3.

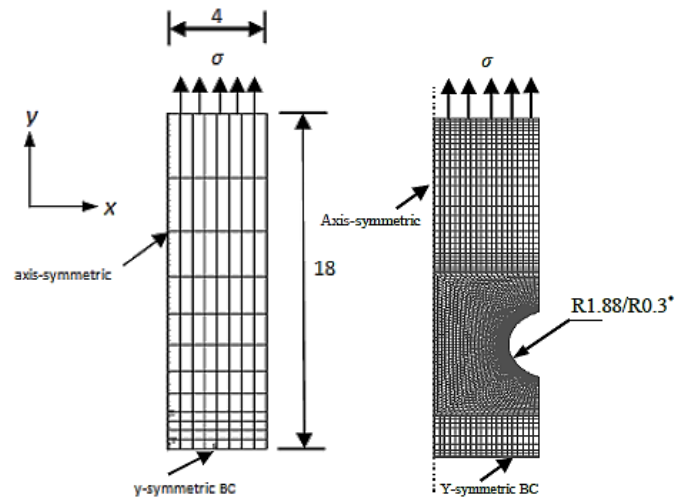


Fig. 3 - Finite element model for smooth and double-notches bar specimen

3. Results and Discussion

3.1 Creep Rupture of Plain Specimen

The rupture time of Grade 91 steel for smooth and notched bar specimens was numerically predicted. The damage was calculated separately, first is using the MG failure strain and secondly using strain at fracture. Fig. 4(a) shows the comparison of FE prediction curve obtained using both parameters against experimental data [16]. Clearly, the FE prediction curves fall on the experimental data indicating the accuracy in predicting the rupture time at short and longer creep time under uniaxial stress state. It is worth to note that the rupture time is estimated when the damage is fully developed across the notch plane. Also shown in this figure is the creep strength breakdown or transition point between short- and long-term creep regimes which occurs at half of 0.2% offset yield stress (~125 MPa). Note that the scatter in the experimental data is due to different heat treatment/cast and the raw material form (pipe, tube and plate) to extract the specimen.

The other form of plot to compare rupture life between experimental data and FE prediction is also shown in Fig. 4(b). Accounting the level of scatter of rupture data, only few data falls outside the region of \pm factor of 2 from 1:1 ratio prediction line ($t_{f(\text{exp})} = t_{f(\text{prediction})}$). Overall, the prediction method predicts well the rupture life of the material under uniaxial stress state. Further evaluation on the feasibility of MG strain in predicting creep life under multiaxial stress state is performed and presented in the following section.

3.2 Creep Rupture of Notched Bar

A total of five notched bar specimen with two acuity ratio (net diameter, d /notch radius, r) of 3.0 and 20 were modelled in FE software. The stress applied to the specimen is chosen following the experimental data [13]. Fig. 5 compares the result of rupture time between FE and experimental data under different acuity/constraint levels. By employing the MG failure strain, all the predicted points of acuity 3.0, (except for one point), fall on the middle line which indicates a good agreement is obtained between FE and experiment data. At the net stress, $\sigma_n = 202$ MPa, the FE underestimates the rupture time, however, is still within the lower bound (-ve factor of 2). The prediction using the strain at fracture is also included in Fig. 6 to allow a direct comparison between the two approaches. In general, a conservative prediction is obtained using the strain at fracture. Highest conservatism can be seen at stress level of 202 MPa where the FE prediction falls outside the upper/lower bound line.

Only one notched bar specimen with acuity of 20 (high constraint) is modelled in FE software due to the unavailability of data. For this acuity level, both approaches predict well the rupture time of the material. Obviously, utilizing MG failure strain into equation (5) resulted conservative prediction than using the strain at fracture. At this point, the conclusion on the suitability of the MG fracture strain to predict the failure of the material under high constraint conditions cannot be made as the available data assessed is very limited. Further investigation could be made when more data becomes available.

3.3 Stress Distribution and Creep Damage

The von-Mises and equivalent creep strain along the notch throat are explored to better understand the rupture and damage behavior under multiaxial stress state features. The von-Mises stress was shown to govern the deformation and creep voids nucleation process [21]. As seen in Figs. 6 and 7, the von-Mises is non uniform, with the maximum stress localized near to the notch root. The stress is steadily decreasing in the direction towards the notch center. Also shown in

the figures is the equivalent creep strain distribution. Clearly, the creep strain distribution shows similar trend as von-Mises stress. For sharp notch specimen, the equivalent creep strain value remains at small value (~ 0) except at the notch root. Later, it will be shown that the damage initiation point does not occur at the same location as maximum equivalent creep strain. Since the value of critical strain is affected by the constraint/triaxiality (higher triaxiality leads to lower critical strain), the damage can occur at the point where the creep strain is not a maximum, depending on the triaxiality value. The location of damage initiation thus is determined based on the competition between equivalent creep strain and triaxiality.

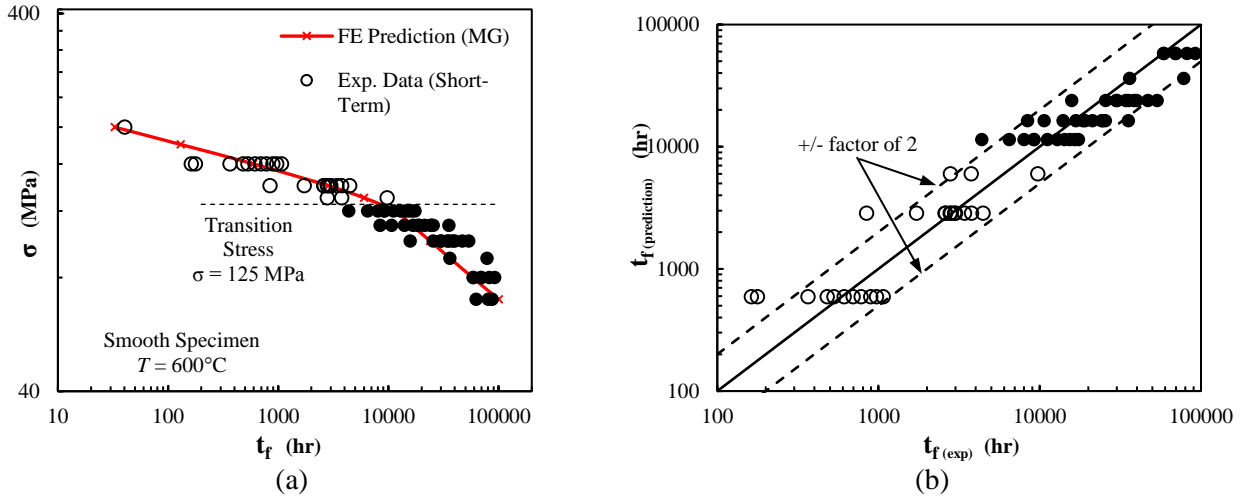


Fig. 4 - Comparison between FE predicted and experimental data of rupture life

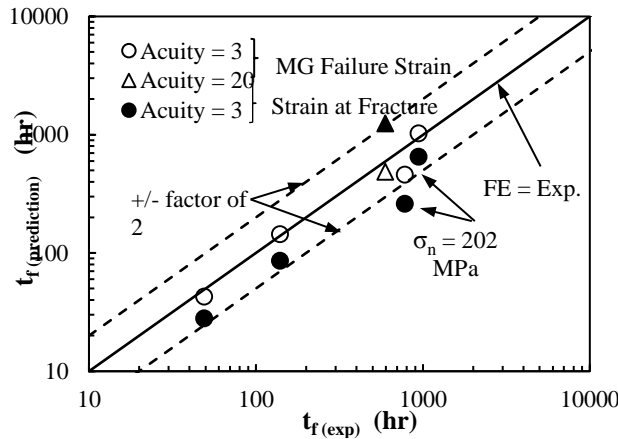


Fig. 5 - Comparison between FE predicted and experimental of the notched bar

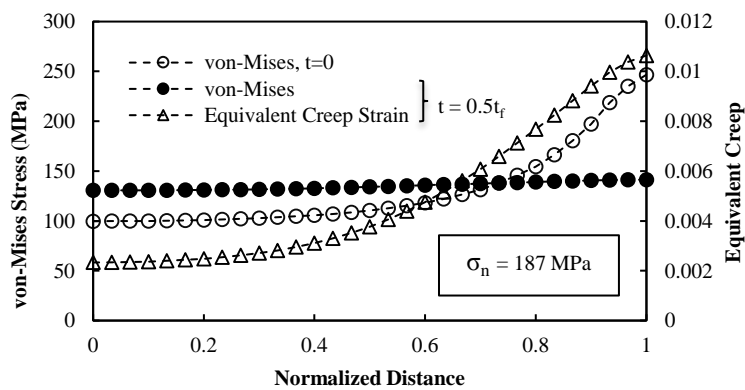


Fig. 6 - von-Mises and equivalent creep strain distribution for notched bar (acuity = 3.0)

According to Cock and Ashby void growth model in equation (6), it is implicitly suggested that the material with high triaxiality ratio tends to fracture in brittle manner. The material or component with low triaxiality factor, in contrast, tends to fracture in ductile means. In other word, triaxiality controls the reduction in creep strain of the material. Fig. 8 shows the plot of notch acuity against triaxiality factor between $t/t_f = 0$ to $t/t_f = 0.5$. Clearly, the triaxiality factor of the high acuity samples is greater than that of the low acuity. Consequently, brittle fractures are commonly observed. The occurrence is consistent with what has been observed in the literature [18]. For the blunt sample, the location of highest triaxiality value is found between the notch center and the root, but for the sharp sample, the maximum triaxiality is found adjacent to the notch tip. Interestingly, the triaxiality ratio along the notch throat plane remains unchanged over the time. Also observed in the Fig. 8 is that, regardless of notch geometry, the triaxiality factor has its lowest value at the notch root.

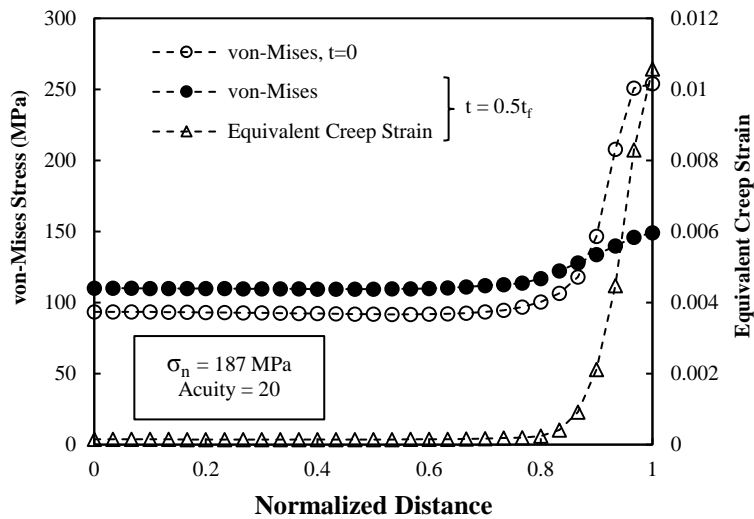


Fig. 7 - von-Mises and equivalent creep strain distribution for notched bar (acuity = 3.0)

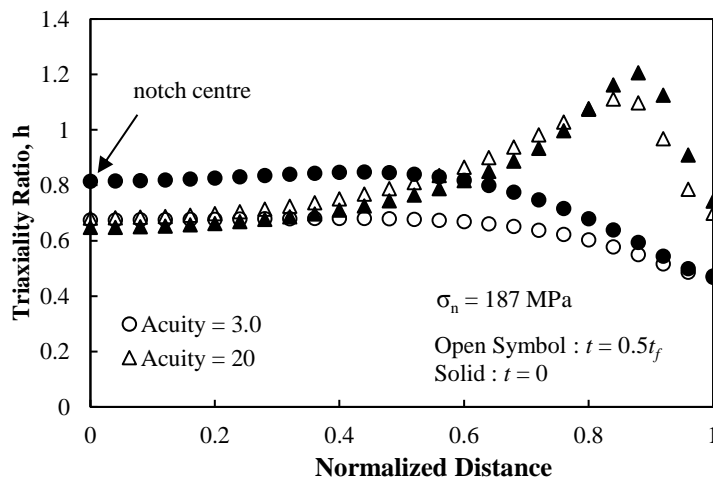


Fig. 8 - Comparison between FE predicted and experimental of notched bar

The variation of damage distribution at different creep time for notched bar under the net stress of 187 MPa is shown in Fig. 9. Based on this figure, it is observed that the sample experiences highest creep damage at the location adjacent to notch tip (at $t = 0.1t_f$). The maximum damage position gradually shifts towards notch center as time passes (see the arrow in Fig. 9(a)). The maximum creep damage finally occurs in between notch center and root. Interestingly, for the sharp notch, the highest damage value remains accumulate near the notch root, indicating that the position of damage is unaffected by time. Comparing between the two acuity levels, the damage extends to a wider area for the low acuity specimen but relatively to a narrow area for the high acuity specimen. The damage level for the sharp notch remains low at most of the area except at the location close to notch root. The observation is true even when the time approaches rupture time.

The FE simulation result in Fig. 10 shows that the damage initiation for low constraint specimen occurs in between the center and root of the notch. For high constraint specimen, however, the damage initiated at the notch root. Detailed

investigation on the stress distribution at the notch throat revealed that damage is likely to initiate at the location with highest triaxiality stress or equivalent creep strain. Note that maximum creep damage for high acuity specimen remains accumulated (locally) at the notch root. As a result, stable crack propagation is clearly observed before the specimen fractured [13,22,23].

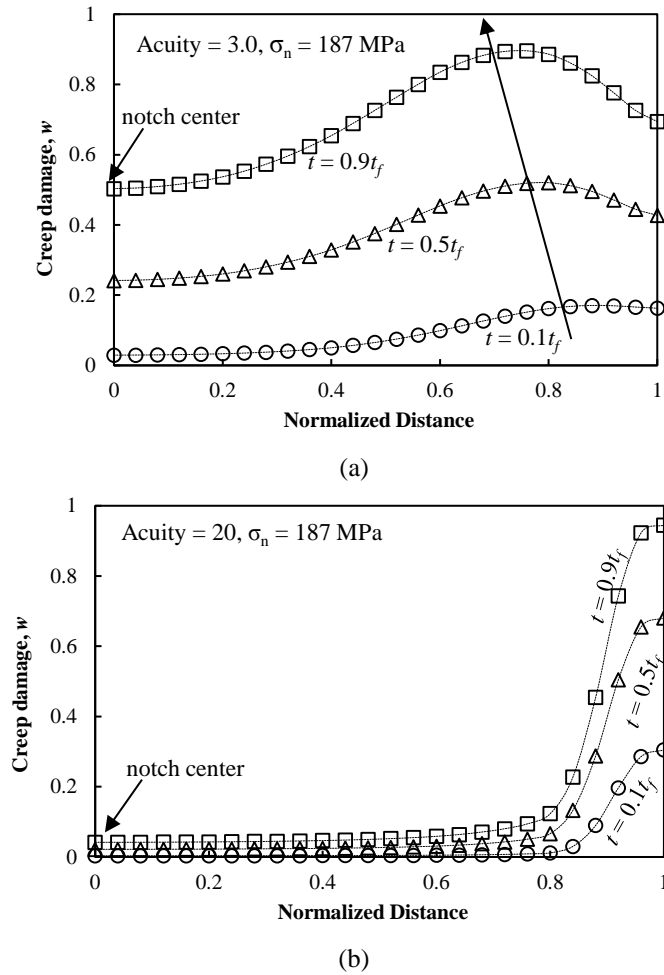


Fig. 9 - Comparison between FE predicted and experimental of notched bar

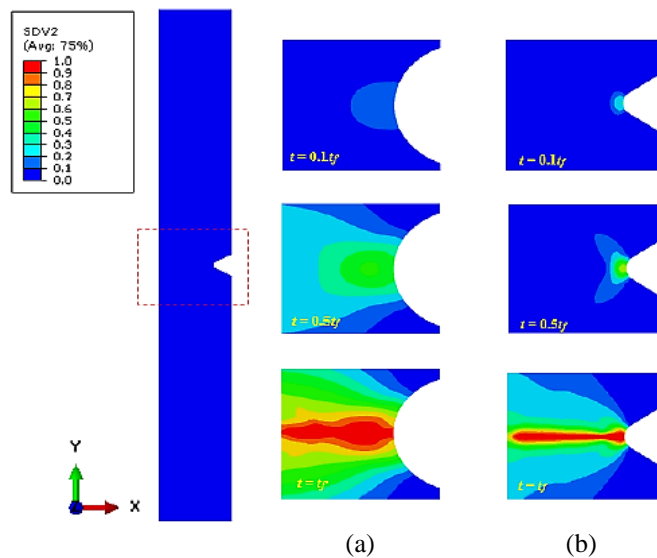


Fig. 10 - Damage evolution at notch area of notched bar (a) acuity 3.0; (b) acuity 20

4. Conclusion

MG failure strain has been numerically evaluated as a key parameter in damage model. The creep rupture time under uniaxial and multiaxial stress state condition has been estimated. The notch acuity appears to effect the position of creep damage initiation. For the case of high acuity or sharp notch, the damage initiates at the notch root. As the acuity decreases, it moves towards the notch's center. Furthermore, it is discovered that at high stress and low acuity, a rupture-type fracture is dominated while at low stress and high acuity, stable crack propagation occurs before the fracture takes place. Overall, employing MG strain into the ductility exhaustion damage model predicts the rupture life well. It has been demonstrated that MG failure strain can be employed as an alternative to strain at fracture. MG strain outweighs strain at fracture because its value can be measured once the secondary creep is established. Unlike strain at fracture, determination of MG failure strain only required short-term testing.

Acknowledgment

The authors would like to express their gratitude and thanks to Ministry of Higher Education (MOHE) Malaysia for providing financial support under Fundamental Research Grant Scheme FRGS/1/2019/TK03/UMP/02/2 (University reference RDU1901107) and Universiti Malaysia Pahang for laboratory facilities and additional funding under Internal Grant RDU1803135.

References

- [1] Lee, J.S., Armaki, H.G., Maruyama, K., Muraki, T., Asahi, H. (2006). Causes of breakdown of creep strength in 9Cr–1.8W–0.5Mo–VNb steel, *Mater. Sci. Eng. A*, 428(1), pp. 270–5
- [2] Hyde, T.H., Sun, W., Becker, A.A. (2005). Use of life and strain fraction rules for creep life prediction of pressurized pipe components undergoing geometry change, *J. Strain Anal. Eng. Des.*, 40(4), pp. 385–94
- [3] Christopher, J., Sainath, G., Srinivasan, V.S., Samuel, E.I., Choudhary, B.K., Mathew, M.D., Jayakumar, T. (2013). Continuum Damage Mechanics Approach to Predict Creep Behaviour of Modified 9Cr-1Mo Ferritic Steel at 873K, *Procedia Eng.*, 55, pp. 798–804
- [4] D.R Hayhurst, R..J Hayhurst and F. Vakili-Tahami (2005). Continuum damage mechanics predictions of creep damage initiation and growth in ferritic steel weldments in a medium bore branched pipe under constant pressure at 590 °C using a five-material weld model, *Proceeding R. Soc. A*, 461(2060)
- [5] Saber, M. (2011). Experimental and finite element studies of creep and creep crack growth in P91 and P92 weldments. University of Nottingham, 2011
- [6] Alang, N.A., Razak, N.A. (2019). Application of ductility exhaustion based damage model to predict creep rupture time of grade 92 steel, *{IOP} Conf. Ser. Mater. Sci. Eng.*, 670, pp. 12001
- [7] Quintero, H., Mehmanparast, A. (2016). Prediction of creep crack initiation behaviour in 316H stainless steel using stress dependent creep ductility, *Int. J. Solids Struct.*, 97–98, pp. 101–15
- [8] Spindler, M.W., Hales, R., Skelton, R.P. (2001). Multiaxial creep ductility of an ex-service type 316 H stainless steel. 9th Int. Conf. on Creep and Fract. of Eng. Mater. and Struct., IOM, pp. 679–88
- [9] Rice, J.R., Tracey, D.M. (1969). On the ductile enlargement of voids in triaxial stress fields*, *J. Mech. Phys. Solids*, 17(3), pp. 201–17
- [10] Cocks, A.C.F., Ashby, M.F. (1980). Intergranular fracture during power-law creep under multiaxial stresses, *Met. Sci.*, 14(8–9), pp. 395–402
- [11] Alang, N.A., Nikbin, K. (2018). An analytical and numerical approach to multiscale ductility constraint based model to predict uniaxial/multiaxial creep rupture and cracking rates, *Int. J. Mech. Sci.*, 135, pp. 342–52
- [12] Alang, N.A., Nikbin, K. (2019). A new approach to predict creep rupture of Grade 92 steel under multiaxial stress states, *Int. J. Mech. Sci.*, 163, pp. 105096, Doi: <https://doi.org/10.1016/j.ijmecsci.2019.105096>
- [13] Razak, N.A. (2018). Creep and creep-fatigue interaction in new and service exposed P91 steel. Imperial College London, 2018
- [14] Yoshida, K., Yatomi, M. (2011). Creep damage evaluation for HAZ of Mod. 9Cr-1Mo steels under multi-axial stress conditions, *Procedia Eng.*, 10, pp. 490–5
- [15] Jae Jun Han, Han Sang Lee, Yun-Jae Kim, Nak Hyun Kim, Woo Gon Kim, Hyeong Yeon Lee, D.W.J. (2015). Prediction of creep crack initiation and growth for P91 at 600°C using MOD-NSW model, *Strength, Fract. Complex.*, 9(1), pp. 125–36
- [16] NIMS. (2014). 9Cr-1Mo-V-Nb (Tubes, Plates and Pipe), Creep data sheet No. 43A,
- [17] Kimura, K., Sawada, K., Kushima, H. (2010). Long-term creep strength property of advanced ferritic creep resistant steels. *Advanced in Material Technology for Fossil Power Plants*
- [18] Nikbin, K. (2017). A unified multiscale ductility exhaustion based approach to predict uniaxial, multiaxial creep rupture and crack growth, *Eng. Fract. Mech.*, 179, pp. 240–59
- [19] Alang, N.A. (2018). Prediction of long-term static and cyclic creep rupture and crack growth of grade 92 steels

- under different stress states. Imperial College London, 2018
- [20] Wen, J.-F., Tu, S.-T., Xuan, F.-Z., Zhang, X.-W., Gao, X.-L. (2016). Effects of Stress Level and Stress State on Creep Ductility: Evaluation of Different Models, *J. Mater. Sci. Technol.*, 32(8), pp. 695–704
 - [21] Nix, W.D., Earthman, J.C., Eggeler, G., Ilschner, B. (1989). The principal facet stress as a parameter for predicting creep rupture under multiaxial stresses, *Acta Metall.*, 37(4), pp. 1067–77
 - [22] Zhao, L., Alang, N., Nikbin, K. (2018). Investigating creep rupture and damage behaviour in notched P92 steel specimen using a microscale modelling approach, *Fatigue Fract. Eng. Mater. Struct.*, 41(2), pp. 456–72
 - [23] Panait, C. (2010). Metallurgical evolution and creep strength of 9-12% Cr heat resistant steels at 600°C and 650°C. L'Ecole Nationale Supérieure Des Mines de Paris, 2010